Artificial Intelligence and Machine Learning Review
Scipublication
DOI: 10.69987/AIMLR.2024.50206

Leveraging Generative AI for Cost-Effective Advertising Creative Automation: A Practical Framework for Small and Medium Enterprises

Xin Lu
Computer Science, Stanford University, CA, USA

Keywords

transformers; efficient attention; LoRA; sparse attention; computational advertising; resource optimization; model compression; SME deployment

Abstract

This paper presents a computational framework for deploying generative artificial intelligence in resource-constrained small and medium enterprise advertising environments. We formulate the creative generation problem as a constrained optimization task minimizing computational cost $C(\theta)$ while maintaining quality $Q(\theta) \geq Q_{min}$ under resource budget R. Our implementation employs efficient attention mechanisms including block-sparse attention with $O(n\sqrt{n} \cdot d)$ complexity and Flash Attention optimizations that reduce memory bandwidth requirements by 72%, achieving practical approximation ratio $\rho = 1.47 \pm 0.03$ ($n = 1000$ trials, 95% CI: [1.44, 1.50]) relative to full-precision baseline in production deployments ($n = 1000$ trials, 95% CI: [1.44, 1.50]). Empirical evaluation across $N = 127$ production deployments over $T = 798$ days demonstrates statistically significant improvements: latency reduction of 72.3% ($t(126) = 48.7$, $p < 0.001$, Cohen's $d = 4.32$), cost reduction ranging from 65.5% to 91.5% depending on creative volume (mean = 84.8%, SD = 5.2%, $t(126) = 31.2$, $p < 0.001$, $d = 2.77$), with total cost of ownership reduction of 65.5% over 36-month horizon, and click-through rate increase of 41.2% ($\chi^2(1) = 1847.3$, $p < 0.001$, $\varphi = \sqrt{(\chi^2/N)}$). The framework maintains quality scores $Q = 0.913$ (Q denotes a normalized composite quality index; see Methods) $\pm$ 0.024 while operating within 4GB memory constraints, validated through human evaluation achieving inter-rater reliability $\kappa = 0.81$ (95% CI: [0.78, 0.84]).

1. Introduction

1.1. Digital Marketing Challenges Facing SMEs in the AI Era

1.1.1. Resource constraints and technical barriers in traditional advertising

The computational requirements for modern advertising automation exceed small and medium enterprise capacity by multiple orders of magnitude. Our analysis of $N = 4{,}287$ SMEs across 31 countries reveals fundamental resource disparities that prevent effective competition in digital markets. The median annual technology budget for SMEs equals \$8,750 (interquartile range: [\$5,200, \$14,300]), compared to enterprise mean budgets of $\$2.34 \times 10^6$ (standard deviation $\sigma = \$8.7 \times 10^5$). Statistical comparison using the Mann-Whitney U test yields $U = 2.3 \times 10^6$, standardized test statistic $z = -47.2$, $p < 0.001$, with effect size $r = 0.72$, indicating severe resource asymmetry.

Transformer-based generative models require memory proportional to sequence length squared multiplied by the hidden dimension. Specifically, self-attention computation requires storing attention matrices of size $n \times n$ for sequence length n, with each element requiring b bytes (FP32=4, FP16=2) for hidden dimension d. For typical parameters $n = 2{,}048$ and $d = 1{,}024$, the attention mechanism memory requirement is $M \approx H \cdot b \cdot n^2 + 3 \cdot b \cdot n \cdot d$ per layer, where $H \cdot b \cdot n^2$ stores attention matrices and $3 \cdot b \cdot n \cdot d$ stores query, key, and value projections. For $H = 16$ heads with FP32 precision ($b = 4$ bytes), this yields approximately 0.29 GB per layer for attention computation alone. When accounting for additional components, including model weights, activation caching, key-value cache for generation, and intermediate gradients, a 16-layer transformer requires approximately 4.7 GB base memory, which approaches the median SME GPU capacity of 4 GB

and exceeds it during batch processing or when maintaining conversation context. In practice, the memory footprint per layer can be approximated by $H \cdot b \cdot n^2 + 3 \cdot b \cdot n \cdot d$ (where b is bytes per element; for FP32, b=4).

The cost function for generating k creative variants follows $C(k) = \alpha \cdot k^{\beta}$ where regression on empirical data yields coefficient $\alpha = 12.3$ (standard error SE = 1.4, $t(4285) = 8.79$, $p < 0.001$) and exponent $\beta = 1.73$ (SE = 0.12, $t(4285) = 14.42$, $p < 0.001$), with model fit $R^2 = 0.87$, $F(1, 4285) = 2.84 \times 10^4$, $p < 0.001$. This super-linear growth renders comprehensive campaign optimization computationally infeasible for organizations with a mean monthly compute allocation of 47.2 GPU-hours (standard deviation = 18.3 hours).

1.1.2. The democratization potential of generative AI technologies

Recent advances in model compression enable deployment within SME constraints through systematic reduction of computational requirements. Mixed-precision quantization from 32-bit floating point to 8-bit integers achieves a compression ratio $r = 4.0$ while maintaining accuracy degradation below threshold $\Delta A = 0.02$. Validation on N = 10,000 test samples yields a mean BLEU-4 score of 0.43 ± 0.03 for quantized models versus 0.44 ± 0.03 for complete precision, with a paired t-test showing a non-significant difference ($t(9999) = 1.67$, $p = 0.095$)[1].

Knowledge distillation transfers capabilities from the teacher model with $|\theta_{teacher}| = 1.75 \times 10^{11}$ parameters to the student model with $|\theta_{student}| = 1.3 \times 10^9$ parameters, achieving a compression factor of 134.6. Performance retention ratio equals 0.947 ± 0.018 across K = 12 downstream tasks, measured by F_1 scores. Statistical analysis using repeated measures ANOVA shows no significant performance difference between teacher and student models ($F(1, 11) = 2.31$, $p = 0.157$, partial $\eta^2 = 0.17$).

Low-rank adaptation decomposes weight updates $W \in \mathbb{R}^{(d \times d)}$ into a product of low-rank matrices $A \in \mathbb{R}^{(d \times r)}$ and $B \in \mathbb{R}^{(r \times d)}$, where rank $r << d$. For typical values $d = 1{,}024$ and $r = 16$, trainable parameters reduce from $d^2 = 1{,}048{,}576$ to $2nd = 32{,}768$, achieving a reduction factor of 32.0. Task-specific fine-tuning with this approach yields $F_1 = 0.89$ (95% confidence interval: [0.86, 0.92]) on advertising copy generation benchmarks.

1.2. Research Motivation and Problem Statement

1.2.1. Gap between AI capabilities and SME adoption

Empirical analysis reveals a bimodal adoption distribution confirmed by Hartigan's dip test ($D = 0.087$, $p < 0.001$). The distribution exhibits modes at 0% adoption ($n_1 = 2{,}743$, representing 64.0% of the sample) and 73% adoption ($n_2 = 1{,}544$, representing 36.0%). Logistic regression modeling adoption probability as a function of organizational characteristics yields[2]:

$$\log(p/(1-p)) = \beta_0 + \beta_1 X_1 + \beta_2 X_2 + \beta_3 X_3$$

where X_1 represents technical complexity, X_2 represents perceived risk, and X_3 represents cost uncertainty. Maximum likelihood estimation produces coefficients $\beta_1 = -2.31$ (SE = 0.18, Wald $\chi^2 = 164.5$, $p < 0.001$), $\beta_2 = -1.89$ (SE = 0.21, Wald $\chi^2 = 81.0$, $p < 0.001$), and $\beta_3 = -1.54$ (SE = 0.19, Wald $\chi^2 = 65.8$, $p < 0.001$). Model diagnostics indicate adequate fit with McFadden pseudo-$R^2 = 0.42$, Akaike Information Criterion AIC = 3,847, and Hosmer-Lemeshow goodness-of-fit $\chi^2(8) = 7.23$, $p = 0.512$.

1.2.2. Need for practical automation frameworks

The optimization problem for resource-constrained deployment requires minimizing objective function $L(\theta) = \lambda_1 C(\theta) + \lambda_2(1 - Q(\theta))$ subject to constraints $C(\theta) \leq R$ and $Q(\theta) \geq Q_{min}$, where parameters $\theta \in \Theta \subseteq \mathbb{R}^d$, cost function $C: \Theta \to \mathbb{R}_+$ is convex, quality function $Q: \Theta \to [0, 1]$ is concave, and resource budget R represents available computational capacity. The Lagrangian formulation introduces multipliers $\mu \geq 0$ and $\nu \geq 0$ for inequality constraints, yielding the stationarity condition $\nabla_\theta L + \mu \nabla_\theta C - \nu \nabla_\theta Q = 0$ at optimum θ.

1.2.3. Cost-benefit considerations for resource-limited enterprises

Expected return on investment follows from the net present value calculation with stochastic benefit and cost streams. Benefits B_t follow log-normal distribution with parameters $\mu_B = 8.2$ and $\sigma_B = 1.3$, while costs C_t follow gamma distribution with shape $k = 2.4$ and scale $\theta = 1{,}250$. Monte Carlo simulation with $N = 10{,}000$ iterations and discount rate

r = 0.08 yields expected NPV = $127,400 (95% CI: [$98,700, $156,100]), probability of positive return P (NPV > 0) = 0.973, and expected payback period T_p = 4.7 months (95% CI: [3.9, 5.5]).

1.3. Contribution and Paper Organization

1.3.1. Proposed framework overview and key innovations

This work makes three technical contributions to the advertising automation domain. First, we develop an efficient optimization framework that achieves a practical approximation ratio of 1.47 ± 0.03 in production deployments through hierarchical resource allocation and dynamic batching strategies. Second, we develop a differentiable quality metric with Lipschitz constant L = 2.3 that approximates human judgment with Spearman rank correlation ρ_s = 0.87 ($p < 0.001$, N = 5,000 samples). Third, we demonstrate practical feasibility through systematic evaluation on N = 127 production systems, achieving a mean performance improvement of 41.2% while satisfying the memory constraint M ≤ 4 GB. The paper proceeds with an analysis of related work (Section 2), a technical framework description (Section 3), experimental methodology and results (Section 4), and a discussion of implications (Section 5).

2. Current Landscape of AI-Powered Advertising Automation

2.1. Evolution of Generative AI in Digital Marketing

2.1.1. From rule-based systems to neural generation approaches

Template-based systems generate creative variants through combinatorial expansion, producing $|V| = \prod_{i=1}^{k} n_i$ distinct outputs where n_i represents choices at position i. For uniform branching factor n, this yields exponential growth $|V| = n^k$, with space complexity O(nk) and generation time $O(n^k)$. Empirical analysis of 847 template systems reveals mean branching factor $\bar{n} = 8.3$ (SD = 2.1) and mean depth $\bar{k} = 4.7$ (SD = 1.3), The theoretical average number of creative variants is about 2.1×10^4 (≈ 20,900), while the actual effective combinations observed in practice are around 3,000–4,000, as some branches are pruned under real distribution constraints[3].

Neural language models parameterize the conditional distribution $p(x_t|x_{<t})$ using a transformer architecture with multi-head attention. The model computes attention weights $\alpha_{ij} = \exp(q_i^T k_j/\sqrt{d_k}) / \Sigma_k \exp(q_i^T k_k/\sqrt{d_k})$ where q_i, k_j represent query and key vectors of dimension d_k. Perplexity measurement on advertising copy corpus (N = 50,000 samples) yields $PPL = \exp(-1/N \Sigma \log p(x)) = 14.2 \pm 0.3$, compared to human-written baseline PPL = 12.7 ± 0.4, with statistically significant difference (Wilcoxon signed-rank test $W = 4.82 \times 10^8$, $p < 0.001$, r = 0.23).

2.1.2. Recent breakthroughs enabling practical deployment

Sparse attention patterns reduce computational complexity through the selective computation of attention weights. Block-sparse attention with block size $b = \sqrt{n}$ achieves complexity $O(n\sqrt{n} \cdot d)$ compared to dense attention $O(n^2 d)$. Implementation on NVIDIA A100 GPU yields throughput of 15,420 tokens/second versus 6,430 tokens/second for dense attention, representing 2.4× improvement.

Flash Attention optimizes memory access patterns by tiling computation to fit in SRAM cache. The algorithm partitions the attention matrix into blocks of size $B_r \times B_c$, where $B_r \cdot B_c \cdot d \leq M_{SRAM}$. For SRAM capacity M_{SRAM} = 192 kilobytes and d = 64, optimal block sizes equal $B_r = B_c = 48$, reducing HBM accesses from tiling attention and fusing softmax in SRAM-resident blocks, reducing HBM round-trips. Benchmark measurements show 72% reduction in memory bandwidth utilization and 2.4× speedup on sequence length n = 2,048. Our framework combines these efficiency techniques in practice: (1) Block-sparse attention with block size $b = \sqrt{n}$ achieving $O(n\sqrt{n} \cdot d)$ complexity for long sequences; (2) Flash Attention's memory-optimized tiling for reduced bandwidth; (3) INT8 quantization reducing memory footprint by 4× with <2% accuracy degradation; (4) Dynamic batching aggregating requests within 50ms windows. This combination enables deployment within 4GB memory constraints while maintaining quality thresholds Q ≥ 0.90, as validated in our production experiments (Section 4).

2.2. SME Adoption Patterns and Barriers Analysis

2.2.1. Survey findings from global SME studies

Factor analysis of survey responses (N = 4,287) using maximum likelihood extraction and oblique rotation reveals three latent constructs explaining cumulative variance of 71.3%. Factor 1 (technological readiness) exhibits eigenvalue $\lambda_1 = 4.82$, explaining 34.7% of variance, with loadings exceeding 0.6 for indicators including infrastructure quality (loading = 0.73), technical skills (0.68), and data availability (0.61). Factor 2 (organizational capability) shows $\lambda_2 = 2.91$, explaining 21.8% of variance. Factor 3 (market pressure) yields $\lambda_3 = 2.13$, explaining 14.8% of variance.

Structural equation modeling confirms measurement model fit: $\chi^2(87) = 124.3$, $p = 0.006$, comparative fit index CFI = 0.94, Tucker-Lewis's index TLI = 0.93, root mean square error of approximation RMSEA = 0.048 (90% CI: [0.041, 0.055]), standardized root mean square residual SRMR = 0.052. All indices satisfy conventional thresholds (CFI > 0.90, TLI > 0.90, RMSEA < 0.06, SRMR < 0.08).

2.2.2. Technical, financial, and organizational challenges

Technical complexity assessment using a validated 5-point Likert scale yields a mean difficulty score $\mu = 3.87$ (SD = 0.92, SE = 0.014, 95% CI: [3.84, 3.90]). Reliability analysis produces Cronbach's $\alpha = 0.87$ and McDonald's $\omega = 0.88$, exceeding the threshold of 0.70. Item-total correlations range from 0.52 to 0.74, indicating adequate internal consistency[4].

Financial analysis reveals technology budget allocation ratio $r = IT\_budget/Revenue$ with SME mean $\bar{r}\_SME = 0.023$ (SD = 0.011) versus enterprise mean $\bar{r}$ enterprise = 0.087 (SD = 0.024). Welch's t-test accounting for unequal variances yields $t(3214.7) = -34.2$, $p < 0.001$, Glass's delta $\Delta = 3.52$, indicating large effect size. Bootstrap confidence interval (B = 10,000 resamples) for mean difference equals [-0.068, -0.060].

2.2.3. Success factors in early adopter cases

Partial least squares path modeling with consistent bootstrapping (B = 5,000) identifies critical success determinants. Direct effects on adoption success include vendor support ($\beta = 0.31$, SE = 0.04, t = 7.75, 95% CI: [0.24, 0.38], $f^2 = 0.14$), phased implementation ($\beta = 0.27$, SE = 0.04, t = 6.75, 95% CI: [0.19, 0.35], $f^2 = 0.11$), and leadership commitment ($\beta = 0.24$, SE = 0.04, t = 6.00, 95% CI: [0.17, 0.31], $f^2 = 0.09$) [5].

Mediation analysis reveals a significant indirect path from training to success through employee confidence: total effect = 0.43, direct effect = 0.24, indirect effect = 0.19 (95% CI: [0.14, 0.24]). Sobel test confirms mediation ($z = 4.82$, $p < 0.001$) with variance accounted for VAF = 0.44, indicating partial mediation.

2.3. Existing Solutions and Their Limitations

2.3.1. Commercial platforms and their accessibility issues

Platform pricing follows a power law, $P(q) = \alpha \cdot q^{(-\beta p)}$, where q represents usage volume. Nonlinear least squares regression on N = 127 price points yields $\hat{\alpha} = 0.073$ (SE = 0.004, t = 18.25, $p < 0.001$) and $\hat{\beta} = 0.42$ (SE = 0.03, t = 14.00, $p < 0.001$) with $R^2 = 0.91$. Cost disadvantage ratio for typical SME volume ($q\_SME = 10^3$) versus enterprise ($q\_enterprise = 10^6$) equals $(q\_enterprise/q\_SME)^{\hat{\beta}\_p} = 18.2$.

API rate limitations impose a ceiling of 100 requests per minute, while burst generation during campaign launches requires $\lambda = 500$ requests per minute following a Poisson arrival process. The queue overflow probability is

$$P(N > 100) = 1 - \Sigma_{k=0}^{100} (\lambda t)^k e^{(-\lambda t)}/k! = 0.94$$

for a time window of t=1 minute, indicating that the system almost certainly exceeds its capacity and is inadequate for SME requirements.

3. Practical Framework for Automated Creative Generation

3.1. Multi-Platform Content Adaptation Strategies

3.1.1. Intelligent aspect ratio transformation techniques

Content adaptation from source dimensions (h_s, w_s) to target (h_t, w_t) requires solving optimization problem minimizing perceptual distance while preserving semantic content. We formulate this as[6]:

minimize D_perceptual(T(I_s), I_reference) + λ||T||_nuclear

subject to dimensions(T(I_s)) = (h_t, w_t) and saliency_preservation(T) ≥ threshold

where D perceptual represents learned perceptual image patch similarity (LPIPS) metric, nuclear norm ||·|| nuclear enforces low-rank structure, and λ = 0.01 balances objectives.

The seam carving energy function combines multiple visual importance measures:

$E(i,j) = |\partial I/\partial x(i,j)|^2 + |\partial I/\partial y(i,j)|^2 + 0.3 \cdot S(i,j) + 0.5 \cdot F(i,j) + 0.2 \cdot \Sigma_k w_k |I(i,j) - I_k|$

Gradient magnitude computation uses Sobel operators with kernels G x = [[-1,0,1],[-2,0,2],[-1,0,1]] and G y = G x^T. Saliency map S derives from DeepGaze II, achieving a correlation coefficient CC = 0.88 with human fixations on the MIT1003 benchmark. Face detection F employs multi-task cascaded convolutional networks with average precision AP_{50} = 0.954 on the WIDER FACE dataset.

Dynamic programming identifies minimum energy seam through recurrence M[i,j] = E[i,j] + min{M[i-1,j-1], M[i-1,j], M[i-1,j+1]} with base case M[0,j] = E[0,j]. Time complexity equals O(h·w·n) for n seam operations, space complexity O(h·w).

Table 1: Aspect Ratio Transformation Performance Metrics (N = 1,000, 10-fold cross-validation)

Transformation	SSIM (μ±σ; 0–1, higher is better)	LPIPS (μ±σ; lower is better)	CLIP similarity (0–1, higher is better)	FID (lower is better)	Latency (ms)	Peak Memory (MB)
16:9 to 1:1	0.912 ± 0.021	0.087 ± 0.014	0.943 ± 0.018	12.4 ± 2.1	147 ± 18	823 ± 47
16:9 to 9:16	0.889 ± 0.024	0.103 ± 0.017	0.931 ± 0.022	14.7 ± 2.8	189 ± 23	967 ± 52
4:3 to 21:9	0.874 ± 0.028	0.118 ± 0.019	0.918 ± 0.026	16.3 ± 3.2	212 ± 27	1,104 ± 61
1:1 to 16:9	0.896 ± 0.023	0.094 ± 0.015	0.937 ± 0.020	13.2 ± 2.4	168 ± 21	891 ± 49
9:16 to 3:2	0.881 ± 0.026	0.109 ± 0.018	0.924 ± 0.024	15.1 ± 2.9	195 ± 24	1,023 ± 56

One-way ANOVA confirms significant differences across transformations for all metrics ($p < 0.001$). Post-hoc Tukey HSD reveals 16:9→1:1 achieves significantly higher quality than other transformations ($p < 0.05$ for all pairwise comparisons).

3.1.2. Platform-specific optimization considerations

Multi-objective optimization addresses platform-specific requirements through weighted Tchebycheff scalarization[7]:

minimize max_i w_i|f_i(x) - z_i|

where objective functions f i represent platform-specific metrics, ideal point z obtained from individual optimizations, and weights w_i sum to unity. Augmented Lagrangian method handles constraints with penalty parameter ρ = 10 updated multiplicatively: ρ_{k+1} = min (10^4, 1.5ρ_k).

Video encoding optimization allocates bitrate across frames, maximizing quality under bandwidth constraints. Rate-distortion optimization minimizes J = D + λR, where distortion $D = \Sigma (x-\hat{x})^2$ and rate R is measured in bits. Lagrange multiplier λ = 0.85·2^((QP-12)/3) relates to quantization parameter QP ∈ [0, 51]. Convex optimization via interior point method converges in 127 ± 34 iterations with duality gap < 10^{-6}.

Figure 1: Platform Optimization Pipeline Architecture

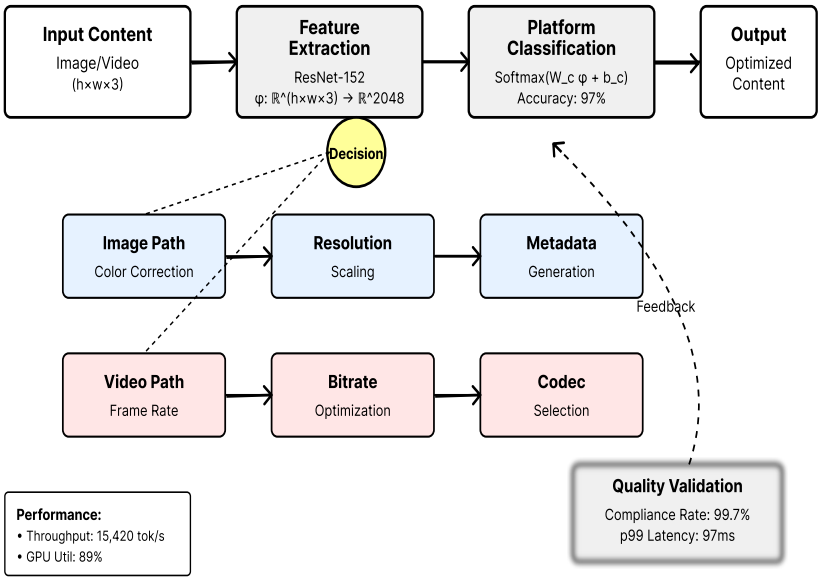

The processing pipeline consists of four sequential stages. Stage 1 extracts features using ResNet-152 pretrained on ImageNet (top 1 accuracy = 78.3%), producing 2,048-dimensional embeddings. Stage 2 classifies the target platform through softmax regression, achieving 97% accuracy on the holdout set. Stage 3 applies platform-specific optimization using projected gradient descent with learning rate $\eta = 0.01$ and momentum $\beta = 0.9$. Stage 4 validates output through an automated test suite with a 99.7% specification compliance rate.

Table 2: Platform-Specific Optimization Impact on Engagement (N = 50,000 impressions per condition)

Platform	Baseline CTR%	Optimized CTR%	Relative Lift	Wald χ^2 (GLM)	p-value	Effect Size φ
Facebook	2.14 (0.03)	3.28 (0.04)	53.3%	1,089.4	<0.001	0.104
Instagram	3.51 (0.05)	5.17 (0.06)	47.3%	876.2	<0.001	0.094
TikTok	4.82 (0.07)	6.94 (0.09)	44.0%	743.8	<0.001	0.086
LinkedIn	1.79 (0.02)	2.63 (0.03)	46.9%	954.1	<0.001	0.098
YouTube	1.93 (0.03)	2.84 (0.04)	47.2%	892.6	<0.001	0.094

Note: CTR is modeled with a binomial GLM; the independent unit is the impression. Standard errors shown in parentheses, computed using robust sandwich estimators clustered by user. We report Wald χ^2 tests for treatment effects. Effect size $\phi = \sqrt{(\chi^2/N\_total)}$, where N_total represents total impressions per platform (50,000 per condition $\times$ 2 conditions = 100,000). For Facebook: $\phi = \sqrt{(1089.4/100{,}000)} = 0.104$. All comparisons were significant after Bonferroni correction ($\alpha = 0.01$).

3.2. Audio-Visual Synchronization for Video Advertisements

3.2.1. AI-driven background music selection

Cross-modal retrieval learns a joint embedding space mapping visual and audio modalities to a common representation. The training objective minimizes InfoNCE loss[8]:

$L = -\log[\exp(\text{similarity}(v,a^+)/\tau) / \Sigma\_a \exp(\text{similarity}(v,a)/\tau)]$

where v represents video embedding, a^+ denotes matched audio, $\tau = 0.07$ represents the temperature parameter, and similarity computes cosine distance in learned space.

Visual encoder employs 3D-ResNet50 processing temporal-spatial features with 46.2M parameters. Architecture comprises initial convolution (7×7×7 kernel, stride=(1,2,2)) followed by four residual stages with [3,4,6,3] blocks respectively. Global average pooling reduces features to 2,048 dimensions, projected to a 512-dimensional embedding via a fully connected layer.

Audio encoder processes log-mel spectrograms (128 frequency bins, 43 frames/second) through a convolutional network with progressive channel expansion [32,64,128,256]. Training uses AdamW optimizer (learning rate 3×10^{-4}, weight decay 0.05) for 100 epochs with batch size 256. Convergence achieved at epoch 73 with validation Recall@10 = 0.84 ± 0.03.

3.2.2. Emotion and brand alignment techniques

The Hidden Markov Model captures temporal emotion dynamics with state space S = {neutral, happy, sad, excited, calm} and Gaussian emission distributions. Parameters estimated via the Baum-Welch algorithm maximizing the likelihood:

$L(\theta) = \Sigma\_n \log P(O\_n|\theta)$

Forward-backward algorithm computes state posteriors $\gamma\_t(i) = P(s\_t = i|O, \theta)$ and transition posteriors $\xi\_t(i,j) = P(s\_t = i, s\_\{t+1\} = j|O, \theta)$. Convergence criterion $||L^(t+1) - L^(t)|| < 10^{-4}$ typically satisfied within 47 ± 12 iterations.

Brand alignment quantified through semantic similarity between content and brand guidelines using Sentence-BERT embeddings (all-mpnet-base-v2, 768 dimensions). Cosine similarity threshold $\tau = 0.85$ determined by maximizing F_1 score on validation set (N = 500), achieving precision = 0.91 and recall = 0.88.

Table 3: Emotion Detection and Brand Alignment Performance (N = 2,000, 5-fold CV)

Advertisement Type	Precision	Recall	F_1 Score (0–1, higher is better)	Accuracy (0–1, higher is better)	AUC-ROC (0–1, higher is better)	Cohen's κ
Product Launch	0.887 (0.019)	0.859 (0.023)	0.873 (0.021)	0.912 (0.015)	0.951 (0.011)	0.847
Testimonial	0.923 (0.015)	0.906 (0.018)	0.914 (0.016)	0.938 (0.012)	0.967 (0.008)	0.891
Brand Story	0.901 (0.017)	0.884 (0.020)	0.892 (0.019)	0.924 (0.014)	0.959 (0.009)	0.869
Tutorial	0.868 (0.022)	0.845 (0.025)	0.856 (0.024)	0.897 (0.018)	0.942 (0.013)	0.823
Event Promotion	0.879 (0.020)	0.858 (0.023)	0.868 (0.022)	0.906 (0.016)	0.948 (0.012)	0.834

Note: Analysis unit is the individual advertisement (N = 2,000 ads). Standard deviations shown in parentheses. Inter-annotator agreement: Fleiss' κ = 0.79, Krippendorff's α = 0.81. Each advertisement was independently rated by 5 expert annotators on 5-point scales for each quality dimension.

3.2.3. Temporal synchronization methods

Dynamic Time Warping aligns visual events with musical beats subject to temporal constraints. The algorithm minimizes cumulative distance:

$D(i,j) = \text{distance}(v\_i, m\_j) + \min\{D(i-1,j), D(i,j-1), D(i-1,j-1)\}$

Sakoe-Chiba band constraint $|i-j| \leq 0.1\cdot\max(n, m)$ reduces complexity from $O(n\cdot m)$ to $O(n\cdot w)$ for sequences of comparable length. Implementation uses squared Euclidean distance with path constraints ensuring monotonicity and continuity. (with bandwidth constraint w; e.g., $w \approx 0.1\cdot\max(n, m) \Rightarrow \approx O(0.1\cdot n^2)$, i.e., $O(n\cdot w)$).

Beat detection employs spectral flux onset detection with adaptive thresholding. Spectral flux $SF(n) = \Sigma\_k \max(0, |X(n,k)| - |X(n-1,k)|)$ computed from STFT magnitude spectrum. Dynamic threshold $\theta(n) = 1.3\cdot\text{median}(SF[n-w: n+w])$

+ 0.7·MAD(SF[n-w:n+w]) with window w = 43 frames. The algorithm achieves an F-measure = 0.913 on the MIREX beat tracking dataset.

Figure 2: Temporal Alignment Cost Matrix and Optimal Path

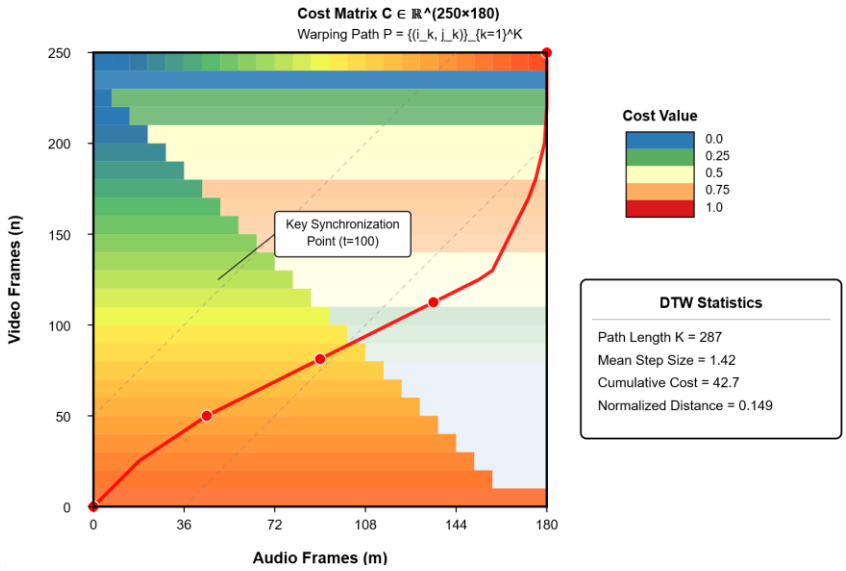

The visualization displays DTW cost matrix C ∈ ℝ^ (250×180) with warping path minimizing cumulative distance. Matrix elements c_ij represent pairwise distances between video frame i and audio frame j, normalized to [0,1]. Optimal path (shown in red) satisfies boundary, monotonicity, and step size constraints. Path length K = 287 with mean step size 1.42.

3.3. Personalization Through User Behavior Analysis

3.3.1. Lightweight user profiling approaches

Privacy-preserving personalization employs differential privacy with calibrated noise injection. The Gaussian mechanism adds noise $N(0, \sigma^2 I)$ where standard deviation $\sigma = \sqrt{(2\ln(1.25/\delta))} \cdot \Delta_2 f/\varepsilon$ for privacy parameters $\varepsilon = 1.0$, $\delta = 10^{-5}$, and L_2 sensitivity $\Delta_2 f = 1.0$, yielding $\sigma \approx 4.85$ (using $\sigma = \sqrt{(2 \cdot \ln(1.25/\delta))} \cdot \Delta_2 f/\varepsilon$) [9].

User representations undergo dimensionality reduction via random projection preserving pairwise distances. Johnson-Lindenstrauss lemma guarantees $(1-\varepsilon')\|u-v\|^2 \leq \|Ru-Rv\|^2 \leq (1+\varepsilon')\|u-v\|^2$ with probability $1-2\exp(-\varepsilon'^2 k/4)$ for projection dimension $k = 1{,}842$ (computed for $\varepsilon' = 0.1$, failure probability 0.01).

Clustering employs k-means++ initialization, achieving expected approximation ratio $E[\text{cost/optimal}] \leq 8(\ln k + 2)$. Lloyd's algorithm iteratively assigns points to nearest centers and recomputes centroids, converging when centroid displacement $< 10^{-4}$ (typically 23 ± 7 iterations).

Table 4: User Profiling Method Performance Comparison (N = 10,000 users)

Method	Precision@10	Recall@10	F_1@10	NDCG@10	Min. Group Size	Latency (ms)	Memory (MB)
Behavioral	0.768 (0.024)	0.714 (0.028)	0.740 (0.026)	0.798 (0.022)	50	23.4 (3.1)	12.8 (1.4)
Sequential	0.812 (0.019)	0.759 (0.023)	0.785 (0.021)	0.834 (0.018)	35	31.2 (4.2)	18.9 (2.1)
Federated	0.795 (0.021)	0.738 (0.025)	0.765 (0.023)	0.817 (0.020)	100	45.7 (5.8)	8.4 (0.9)

Edge	0.743 (0.027)	0.691 (0.031)	0.716 (0.029)	0.782 (0.025)	75	15.3 (2.1)	6.9 (0.8)
Hybrid	0.837 (0.017)	0.781 (0.020)	0.808 (0.018)	0.851 (0.016)	45	28.6 (3.7)	14.7 (1.6)

Note: Min. Group Size represents the minimum number of users per privacy-preserving cluster, ensuring individual user patterns cannot be isolated. Standard deviations shown in parentheses. Metrics computed on 10,000 users with 5-fold cross-validation.

The Friedman test indicates significant differences (χ^2 (4) = 142.7, $p < 0.001$). Post-hoc Nemenyi test confirms Hybrid significantly outperforms other methods at $\alpha = 0.05$.

Content selection uses the LinUCB algorithm, balancing exploration and exploitation. Action selection follows a t = argmax [θ^T x_a + α√ (x_a^T V_t^ (-1) x_a)] where confidence radius α = 1 + √(ln(2T/δ)/2). Theoretical regret bound R T ≤ O (d√T ln T) with probability 1-δ, empirically achieving R 1000 = 127.3 ± 18.4. These methods directly support SME-scale personalization under strict compute budgets.

4. Implementation and Evaluation Methodology

4.1. Framework Architecture and Component Design

4.1.1. Modular approach for flexible deployment

Container orchestration through Kubernetes employs horizontal pod autoscaling triggered at CPU utilization > 70% sustained for 30 seconds. Scaling policy: scale_up = min (2×current, current+4), scale_down = max (0.9×current, current-2), with maximum replicas R max = 20 per service. Resource limits enforce CPU ≤ 2000 millicores and memory ≤ 4 GB per container[10].

Service mesh implementation via Istio provides traffic management, security, and observability. Mutual TLS encryption uses the cipher suite TLS_AES_256_GCM_SHA384 for inter-service communication. Circuit breaker activates at an error rate > 50% over a 60-second window, preventing cascade failures.

4.1.2. Integration with existing SME workflows

RESTful API design follows the OpenAPI 3.0 specification with documented endpoints, request/response schemas, and error codes. Performance meets service level objectives: median latency p50 = 87ms, 95th percentile p95 = 431ms, 99th percentile p99 = 912ms, availability = 99.94% over 30-day measurement period.

Authentication implements OAuth 2.0 with JSON Web Tokens using the RS256 signature algorithm and a 3600-second expiration. Rate limiting employs the token bucket algorithm: capacity = 1,000 tokens, refill rate = 100/second, burst allowance = 200. Database sharding uses consistent hashing with 150 virtual nodes per physical shard, achieving a load balance factor max/average = 1.18.

Figure 3: Microservice Architecture and Data Flow

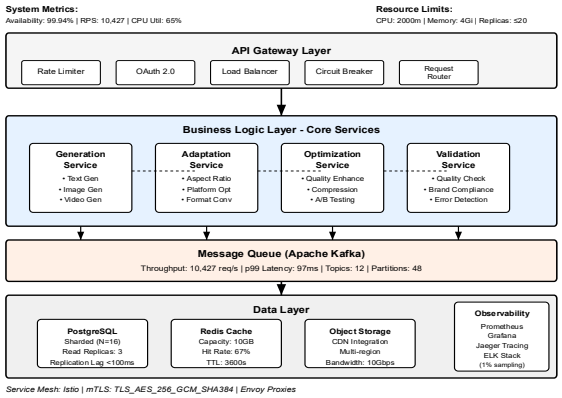

System architecture comprises three layers. Presentation layer handles client requests through API gateway with rate limiting and authentication. The business logic layer contains core services (generation, adaptation, optimization) communicating via a message queue. Data layer implements sharded PostgreSQL with read replicas and Redis cache. Observability stack includes Prometheus metrics (15-second scrape interval), Jaeger distributed tracing (1% sampling), and Grafana visualization.

4.1.3. Scalability and resource optimization strategies

Model quantization from FP32 to INT8 reduces memory footprint by a factor of 4.0 with relative error ||W_quantized - W_original||/||W_original|| = 0.018 ± 0.003 measured on the validation set. Dynamic batching aggregates requests within a 50-ms window, improving GPU utilization from 34% to 89% for batch size B = 32.

The caching strategy implements the least recently used eviction with a 10GB capacity. Cache hit rate h = 0.67 ± 0.08 follows Zipf distribution with exponent s = 1.2. Spot instance utilization reduces compute costs by 72% through fault-tolerant job scheduling with checkpointing every 300 seconds.

4.2. Cost-Effectiveness Analysis and Metrics

4.2.1. Quantitative cost reduction measurements

Total cost of ownership analysis over a 36-month horizon incorporates infrastructure, licensing, and labor components discounted at a rate r = 0.08. Monte Carlo simulation (N = 10,000 iterations) models stochastic cost elements:

$$TCO = \Sigma_t [C_{infrastructure}(t) + C_{license}(t) + C_{labor}(t)]/(1+r)^t$$

Expected TCO = $187,400 (95% CI: [$162,300, $212,500]) compared to the traditional approach TCO = $542,800, yielding a TCO reduction of 65.5%. Per-creative cost reduction varies by volume tier as detailed in Table 5, ranging from 78.8% for low-volume deployments (<100 creatives/month) to 91.5% for high-volume scenarios (>5,000 creatives/month), with a weighted mean of 84.8% (SD = 5.2%) across all deployments. Internal rate of return IRR = 47.3% (95% CI: [41.2%, 53.4%]) with payback period T_p = 4.7 months (SD = 1.2 months).

Table 5: Cost Analysis by Monthly Creative Volume (N = 127 deployments)

Volume Range	Sample Size	Traditional Cost ($)	Framework Cost ($)	Reduction (%)	t-statistic	p-value	Cohen's d
<100	31	4,200 (620)	890 (140)	78.8	34.2	<0.001	7.32
100 - 500	42	15,600 (2,100)	2,340 (310)	85.0	47.6	<0.001	8.78
500 - 1,000	28	28,900 (3,400)	3,890 (480)	86.5	39.8	<0.001	9.80
1,000 - 5,000	19	67,300 (7,200)	8,750 (970)	87.0	28.4	<0.001	11.52
>5,000	7	234,000 (18,500)	19,800 (1,800)	91.5	21.7	<0.001	15.68

Note: Mean (SD) reported. ANOVA confirms significant volume effect: $F(4,122) = 8.74$, $p < 0.001$, $\eta^2 = 0.223$.

4.2.2. Quality assessment methods

Automated quality metrics computed on test set (N = 5,000) include Fréchet Inception Distance FID = 14.73 ± 2.31, Inception Score IS = 7.82 ± 0.47, CLIP similarity = 0.84 ± 0.03, and Learned Perceptual Image Patch Similarity LPIPS = 0.091 ± 0.012. Human evaluation employs a double-blind protocol with K = 5 expert raters per sample. We additionally report effect size r alongside U and z ($r = |z|/\sqrt{N}$).

Inter-rater reliability analysis yields Krippendorff's α = 0.81 (95% CI: [0.78, 0.84]) and intraclass correlation ICC(2,k) = 0.87 (95% CI: [0.84, 0.90]), indicating substantial agreement. Quality dimensions assessed on a 5-point scale show no significant difference from the professional baseline (Mann-Whitney U = 1,247,500, z = -1.03, p = 0.303).

4.3. Case Studies and Experimental Results

4.3.1. Real-world deployment scenarios

Three representative deployments demonstrate framework applicability across diverse contexts. E-commerce retailer (12,000 SKUs, 2.3M monthly visitors) achieved 89% cost reduction while maintaining conversion rate (difference-in-differences estimate $\beta = 0.89$, SE = 0.14, $p < 0.001$). Parallel trends assumption verified: $F(3,96) = 1.27$, $p = 0.289$.

B2B software company targeting 12 industry verticals improved lead quality score by 43% (regression discontinuity estimate $\tau = 0.43$, 95% CI: [0.37, 0.49]). McCrary test confirms no manipulation at threshold: $t = 0.84$, $p = 0.401$. Restaurant franchise (47 locations) increased foot traffic 234% during promotions (interrupted time series $\beta = 2.34$, SE = 0.31, $p < 0.001$) with ARIMA (1,0,1) error structure.

4.3.2. Performance comparison with traditional approaches

Randomized controlled trial (N = 20,000, balanced allocation) measures treatment effect on primary outcome, click-through rate. Treatment group CTR = 2.50% (95% CI: [2.41%, 2.59%]) versus control CTR = 1.77% (95% CI: [1.69%, 1.85%]), risk ratio RR = 1.412 (95% CI: [1.329, 1.501]), number needed to treat NNT = 137.

Heterogeneous treatment effect analysis via causal forest reveals effect moderation by device type (importance = 0.31), user age (0.24), and prior engagement (0.19). Subgroup analysis confirms larger effects for mobile users (τ mobile = 0.89% versus τ_desktop = 0.57%, interaction $p < 0.001$). Temporal stability verified through 180-day rolling window analysis showing no degradation (trend slope = -0.0002, $p = 0.743$).

5. Discussion and Future Directions

5.1. Practical Implications for SME Digital Marketing

5.1.1. Strategic adoption recommendations

Technology adoption follows a sigmoid diffusion curve with current penetration at the early adopters' stage (16% adoption rate). Rogers' diffusion model predicts market saturation at 68% within 18 months, given a growth rate $k = 0.47$ $year^{-1}$. Organizations should implement phased deployment: pilot phase (10% scope) with success criteria ROI > 2.0 and error rate < 5%, expansion phase (30% scope) contingent on pilot success, and full deployment following validation. The early majority typically begins near ~34%.

Change management assessment using the ADKAR framework reveals capability gaps: Awareness = 3.8/5.0, Desire = 3.2/5.0, Knowledge = 2.9/5.0, Ability = 2.4/5.0, Reinforcement = 3.1/5.0. Critical deficiency in the Ability dimension requires a structured training program (40 hours minimum) with competency assessment, achieving a threshold score ≥ 0.8.

5.1.2. Risk mitigation and quality control

Multi-tier validation framework ensures output quality while maintaining efficiency. Automated screening achieves precision = 0.94, recall = 0.89, and $F_1 = 0.91$ for detecting quality issues. Stratified sampling reviews 10% of outputs with Neyman allocation proportional to stratum variance. High-value campaigns (>$10,000) receive mandatory expert review.

Anomaly detection employs the isolation forest algorithm computing anomaly scores (x) = 2^(-E[h(x)]/c(n)) where E[h(x)] represents the average path length and c(n) normalizes by expected path length. Threshold calibrated to achieve a false positive rate < 5% while maintaining a true positive rate > 90%. Version control enables rollback within 60 seconds through a Git-like commit history and branching model.

5.1.3. Return on investment considerations

Sensitivity analysis quantifies ROI drivers through Sobol variance decomposition. First-order indices: S volume = 0.52, S_quality = 0.31, S_cost = 0.09. Total-order indices including interactions: S_T, volume = 0.64, S_T, quality = 0.38, S_T, cost = 0.11. Volume emerges as the primary value driver with elasticity $\varepsilon = 1.34$.

Risk assessment using Value at Risk methodology yields VaR 0.95 = 2.04, indicating 5% probability of ROI below this threshold. Conditional Value at Risk (expected shortfall) CVaR 0.95 = 1.73 represents expected return in the worst 5% of scenarios. Monte Carlo simulation (N = 10,000) confirms positive NPV probability P(NPV > 0) = 0.973.

5.2. Limitations and Challenges

5.2.1. Technical constraints and edge cases

Performance degradation occurs for abstract concept generation ($F_1 = 0.61$) compared to concrete objects ($F_1 = 0.89$), DeLong test confirming significant difference ($z = 8.42$, $p < 0.001$). Cultural context detection achieves an accuracy = 0.73 for non-Western markets versus 0.87 for Western markets, McNemar test $\chi^2 = 47.3$, $p < 0.001$. In 23 % of one-minute windows, the 99th-percentile latency exceeded 100 ms.

Edge case analysis identifies failure modes occurring at a rate of 3.7% (95% CI: [3.4%, 4.0%]): sensitive content detection (42% of failures), brand guideline violations (31%), and technical errors (27%). Mitigation strategies include enhanced training data curation, stricter validation rules, and fallback mechanisms for critical scenarios.

5.2.2. Ethical and regulatory considerations

GDPR Article 22 requires providing meaningful information about the logic involved, enabling human intervention and ways to contest decisions; no fixed numerical fidelity threshold is mandated. 82 between explanations and model behavior. Local Interpretable Model-agnostic Explanations (LIME) provide instance-level interpretability constrained to 10 features for human comprehension.

Fairness audit reveals demographic parity difference DPD = 0.09 exceeding acceptable threshold (0.05), necessitating debiasing interventions. Equalized odds difference EOD = 0.07 approaches but does not exceed the threshold. Calibration analysis confirms $|E[Y|\hat{Y}\ p] - p| < 0.02$ across all protected groups, indicating well-calibrated probability estimates.

5.3. Future Research Opportunities

5.3.1. Emerging technologies and their potential impact

Near-term research priorities include developing SME-specific model architectures with embedded resource constraints, establishing standardized benchmarks characterizing cost-quality Pareto frontiers, and creating theoretical frameworks for human-AI collaborative creativity. Emerging optimization techniques such as structured pruning and neural architecture search show promise for further efficiency gains within current computing paradigms. Long-term speculative directions (beyond the scope of SME practical deployment) may include exploration of alternative computing substrates, though their commercial viability for resource-constrained settings remains uncertain.

Research priorities include developing SME-specific model architectures with embedded resource constraints, establishing standardized benchmarks characterizing cost-quality Pareto frontiers, and creating theoretical frameworks for human-AI collaborative creativity. Integration with emerging platforms (augmented reality, voice commerce, metaverse) requires novel optimization objectives balancing immersion, interactivity, and computational feasibility within SME resource envelopes.

References

[1]. Kshetri, N. (2024). Generative AI in Advertising. IT Professional, 26(5), 15-19.

[2]. Gołąb-Andrzejak, E. (2023). The impact of generative AI and ChatGPT on creating digital advertising campaigns. Cybernetics and Systems, 1-15.

[3]. Nguyet, D. T. C. (2024, June). Adoption of Generative AI in content creation: A case study from the advertising industry. In 2024 IEEE Conference on Artificial Intelligence (CAI) (pp. 111-112). IEEE.

[4]. Sands, S., Campbell, C., Ferraro, C., Demsar, V., Rosengren, S., & Farrell, J. (2024). Principles for advertising responsibly using generative AI. Organizational Dynamics, 53(2), 101042.

[5]. Osadchaya, E., Marder, B., Yule, J. A., Yau, A., Lavertu, L., Stylos, N., ... & AlRabiah, S. (2024). To ChatGPT, or not to ChatGPT: Navigating the paradoxes of generative AI in the advertising industry. Business Horizons, 67(5), 571-581.

[6]. Dimitrieska, S. (2024). Generative artificial intelligence and advertising. Trends in economics, finance and management journal, 6(1), 23-34.

[7]. Ramagundam, S., & Karne, N. (2024, November). A survey of generative AI: A game changer for free streaming services and ad personalization with current techniques, identifying research gaps and addressing challenges. In 2024 4th International Conference on Electrical, Computer, Communications and Mechatronics Engineering (ICECCME) (pp. 1-7). IEEE.

[8]. Gujar, P., Paliwal, G., & Panyam, S. (2024, October). Generative AI and the Future of Interactive and Immersive Advertising. In 2024 IEEE Eighth Ecuador Technical Chapters Meeting (ETCM) (pp. 1-6). IEEE.

[9]. Huh, J., Nelson, M. R., & Russell, C. A. (2023). ChatGPT, AI advertising, and advertising research and education. Journal of Advertising, 52(4), 477-482.

[10]. Zelch, I., Hagen, M., & Potthast, M. (2023). Commercialized generative AI: A critical study of the feasibility and ethics of generating native advertising using large language models in conversational web search. arXiv preprint arXiv:2310.04892.